It is unknown at present why the proliferation-inhibitory effects of tributyltin were not accompanied by the inhibited migration of cNCCs. It is unlikely that tributyltin increased the migration of cNCCs, compensating its proliferation-inhibitory effects. This is because tributyltin did not have any effects on the migration of cNCCs over the concentration tested even when the neural tube was removed at 18 h of culture and the cNCCs could move more freely during the exposure period (data not shown). Rather, the relatively selective toxicity and accumulation of tributyltin in the mitochondria (Doherty & Irwin 2011) might have no effects on the migration of cNCCs. In any case, no correlation between proliferation inhibition and migration inhibition means that the NCC migration assay can not be replaced by usual cytotoxicity assays based on the cell number and is valuable to investigate the effects of chemicals on the function of NCCs.

While valproic acid did not inhibit the migration of cNCCs in the present study, the effects of valproic acid on the migration of NCCs are controversial. Valproic acid inhibited the migration of human NCCs in a scratch assay (Zimmer et al. 2012), but did not inhibit the migration of chick NCCs in cultured neural tubes (Fuller et al. 2002). Currently available data indicate that the effects of valproic acid on the migration of NCCs seem to depend on the assay method and the species used in which it is used.

For other chemicals (acetaminophen, caffeine, and phenytoin) that did not inhibit the migration of cNCCs, no particular information concerning the involvement of NCCs' malfunction in their developmental toxicity was found, except that acetaminophen did not inhibit the migration of human NCCs either (Zimmer et al. 2012).

In conclusion, it was established that several developmentally toxic chemicals inhibit the migration of cNCCs, which appears differently as craniofacial abnormalities. Mechanistic investigation is needed to understand the variability in the outcomes of the

inhibited migration of cNCCs. Our migration assay method will be useful for this purpose because of its simplicity.

CONFLICT OF INTEREST

The authors declare that there are no conflicts of interest.

ACKNOWLEDGEMENTS

This work was supported by a Health and Labor Science Research Grant from the Ministry of Health, Labour and Welfare in Japan.

REFERENCES

Adeeko A, Li D, Forsyth DS, Casey V, Cooke GM, Barthelemy J, Cyr DG, Trasler JM, Robaire B, Hales BF. 2003. Effects of in utero tributyltin chloride exposure in the rat on pregnancy outcome. Toxicol Sci 74: 407–15.

Collins MD, Tzimas G, Hummler H, Bürgin H, Nau H. 1994. Comparative teratology and transplacental pharmacokinetics of all-*trans*-retinoic acid, 13-*cis*-retinoic acid, and retinyl palmitate following daily administrations in rats. Toxicol Appl Pharmacol 127: 132–44.

Cooke GM, Forsyth DS, Bondy GS, Tachon R, Tague B, Coady L. 2008. Organotin speciation and tissue distribution in rat dams, fetuses, and neonates following oral administration of tributyltin chloride. J Toxicol Environ Health A 71: 384–95.

Doherty JD, Irwin WA. 2011. Organotins (tributyltin and triphenyltin). In: Gupta RC, editor. Reproductive and Developmental Toxicology. Sandiego, California: Elsevier. p. 657–672.

Flora SJS, Pachauri V, Saxena G. 2011. Arsenic, cadmium and lead. In: Gupta RC, editor. Reproductive and Developmental Toxicology. Sandiego, California: Elsevier. p. 415–438.

Fuller LC, Cornelius SK, Murphy CW, Wiens DJ. 2002. Neural crest cell motility in valproic acid. Reprod Toxicol 16: 825–839.

Greenaway JC, Mirkes PE, Walker EA, Juchau MR, Shepard TH, Fantel AG. 1985. The effect of oxygen concentration on the teratogenicity of salicylate, niridazole, cyclophosphamide, and phosphoramide mustard in rat embryos in vitro. Teratology 32: 287–295.

Guest I, Buttar HS, Smith S, Varma DR. 1994. Evaluation of the rat embryo culture system as a predictive test for human teratogens. Can J Physiol Pharmacol 72: 57–62.

Gurniak CB, Perlas E, Witke W. 2005. The actin depolymerizing factor n-cofilin is essential for neural tube morphogenesis and neural crest cell migration. Dev Biol 278: 231–241.

Hall BK. 2009. Neurocristopathies. In: The Neural Crest and Neural Crest Cells in Vertebrate Development and Evolution. 2nd ed. New York: Springer. p. 269–293.

Joschko MA, Dreosti IE, Tulsi RS. 1993. The teratogenic effects of salicylic acid on the developing nervous system in rats in vitro. Teratology 48: 104–114.

Kawakami M, Umeda M, Nakagata N, Takeo T, Yamamura K-I. 2011. Novel migrating mouse neural crest cell assay system utilizing P0-Cre/EGFP fluorescent time-lapse imaging. BMC Dev Biol 11: 68.

Kim S-R, Kubo T, Kuroda Y, Hojyo M, Matsuo T, Miyajima A, Usami M, Sekino Y, Matsushita T, Ishida S. 2014. Comparative metabolome analysis of cultured fetal and adult hepatocytes in humans. J Toxicol Sci 39: 717–23.

Kosar K. 1993. Interaction of ibuprofen with early chick embryogenesis. Pharmazie 48: 207–9.

Le Douarin N, Kalcheim C. 1999. The Neural Crest. 2nd ed. New York: Cambridge University Press.

Lee QP, Juchau MR, Kraft JC. 1991. Microinjection of cultured rat embryos: studies with retinol, 13-cis- and all-trans-retinoic acid. Teratology 44: 313–23.

Menegola E, Broccia ML, Di Renzo F, Massa V, Giavini E. 2004. Relationship between hindbrain segmentation, neural crest cell migration and branchial arch abnormalities in rat embryos exposed to fluconazole and retinoic acid *in vitro*. Reprod Toxicol 18: 121–130.

Nakajima M, Mitsunaga K, Nakazawa K, Usami M. 2008. In vivo/in vitro study in rat embryos on indium-caused tail malformations. Reprod Toxicol 25: 426–32.

Robinson JF, van Beelen VA, Verhoef A, Renkens MFJ, Luijten M, van Herwijnen MHM, Westerman A, Pennings JLA, Piersma AH. 2010. Embryotoxicant-specific transcriptomic responses in rat postimplantation whole-embryo culture. Toxicol Sci 118: 675–85.

Rühl R, Plum C, Elmazar MM, Nau H. 2001. Embryonic subcellular distribution of 13-*cis*- and all-*trans*-retinoic acid indicates differential cytosolic/nuclear localization. Toxicol Sci 63: 82–9.

Schardein JL, Macina OT. 2006. Ethanol. In: Human Developmental Toxicants: Aspects of Toxicology and Chemistry. Boca Raton, Florida: Taylor & Francis. p. 301–322.

Shi Y, Li J, Chen C, Gong M, Chen Y, Liu Y, Chen J, Li T, Song W. 2014. 5-mehtyltetrahydrofolate rescues alcohol-induced neural crest cell migration abnormalities. Mol Brain 7: 67.

Shreiner CM, Zimmerman EF, Wee EL, Scott Jr WJ. 1986. Caffein effects on cyclic AMP levels in the mouse embryonic limb and palate in vitro. Teratology 34: 21–27.

Ugwuja EI, Ibiam UA, Ejikeme BN, Obuna JA, Agbafor KN. 2012. Blood Pb Levels in pregnant Nigerian women in Abakaliki, South-Eastern Nigeria. Environ Monit Assess.

Usami M, Mitsunaga K, Irie T, Miyajima A, Doi O. 2014a. Proteomic analysis of ethanol-induced embryotoxicity in cultured post-implantation rat embryos. J Toxicol Sci 39: 285–92.

Usami M, Mitsunaga K, Irie T, Miyajima A, Doi O. 2014b. Simple in vitro migration assay for neural crest cells and the opposite effects of all-trans-retinoic acid on cephalic- and trunk-derived cells. Congenit Anom (Kyoto) 54: 184–188.

Usami M, Mitsunaga K, Nakazawa K, Doi O. 2008. Proteomic analysis of selenium embryotoxicity in cultured postimplantation rat embryos. Birth Defects Res B Dev Reprod Toxicol 83: 80–96.

Usami M, Nakajima M, Mitsunaga K, Miyajima A, Sunouchi M, Doi O. 2009. Proteomic analysis of indium embryotoxicity in cultured postimplantation rat embryos. Reprod Toxicol 28: 477–88.

Weeks BS, Gamache P, Klein NW, Hinson JA, Bruno M, Khairallah E. 1990. Acetaminophen toxicity to cultured rat embryos. Teratog Carcinog Mutagen 10: 361–71.

Wentzel P, Eriksson UJ. 2008. Genetic influence on dysmorphogenesis in embryos from different rat strains exposed to ethanol in vivo and in vitro. Alcohol Clin Exp Res 32: 874–887.

Winn L. 2002. Evidence for Ras-Dependent Signal Transduction in Phenytoin Teratogenicity. Toxicol Appl Pharmacol 184: 144–152.

Yan D, Dong J, Sulik KK, Chen S. 2010. Induction of the Nrf2-driven antioxidant response by tert-butylhydroquinone prevents ethanol-induced apoptosis in cranial neural crest cells. Biochem Pharmacol 80: 144–9.

Zhao SF, Zhang XC, Zhang LF, Zhou SS, Zhang F, Wang QF, Wang YL, Bao YS. 1997. The evaluation of developmental toxicity of chemicals exposed occupationally using whole embryo culture. Int J Dev Biol 41: 275–282.

Zimmer B, Lee G, Balmer N V, Meganathan K, Sachinidis A, Studer L, Leist M. 2012. Evaluation of developmental toxicants and signaling pathways in a functional test based on the migration of human neural crest cells. Environ Health Perspect 120: 1116–22.

Legends to the figures

Fig. 1. Culture schedule of for the migration and proliferation assays of cephalic neural crest cells (cNCCs)

Neural tubes were excised from the rhombencephalic region of day 10.5 rat embryos and cultured for 48 h to allow the emigration of cNCCs. Chemicals were added to the culture medium at 24 h. In the proliferation assay, the neural tubes were removed from the culture dishes at 18h leaving the cNCCs behind, and the cell nuclei were fluorescently stained before the photography at 48 h.

Fig. 2. Photographs of cephalic neural crest cells (cNCCs) cultured in the migration and proliferation assays

(A) cNCCs cultured in the migration assay are shown with blue polygons connecting the outermost cells for the calculation of the cell migration. (B) cNCCs cultured in the proliferation assay are shown with blue dots (24 h) or stained cell nuclei (48 h) for the determination of the cell count.

Fig. 3. Migration of cephalic neural crest cells (cNCCs) cultured in the presence of developmentally toxic chemicals with migration-inhibitory effects

Migration indices were calculated as the radius ratio from the circular spread of cNCCs at 24 and 48 h of culture. The mean ± standard error of the mean (SEM) values of 6–27 neural tubes are shown. Asterisks indicate statistically significant differences from the corresponding control (*, $p < 0.05$; **, $p < 0.01$; ***, $p < 0.001$; ****, $p < 0.0001$).

Fig. 4. Migration of cephalic neural crest cells (cNCCs) cultured in the presence of

developmentally toxic chemicals without migration-inhibitory effects

Migration indices were calculated as the radius ratio from the circular spread of cNCCs at 24 and 48 h of culture. The mean ± standard error of the mean (SEM) values of 8–16 neural tubes are shown. Effects of indium were examined also in trunk neural crest cells as shown in (C).

Fig. 5. Proliferation of cephalic neural crest cells (cNCCs) cultured in the presence of developmentally toxic chemicals

The cNCCs were counted at 24 and 48h of culture, and the proliferation indices were calculated. The mean ± standard error of the mean (SEM) values of 7–10 neural tubes are shown. Asterisks indicate statistically significant differences from the corresponding control (*, $p < 0.05$; **, $p < 0.01$; ***, $p < 0.001$).

Fig. 6. Plot of the reduced migration versus the reduced cell count ratio of neural crest cells cultured in the presence of developmentally toxic chemicals

The reduced migration and reduced cell count ratio were calculated by subtracting the corresponding data in Figs. 1–3 from 100%. The linear regression line and correlation coefficient (r) for all the plotted data are shown.

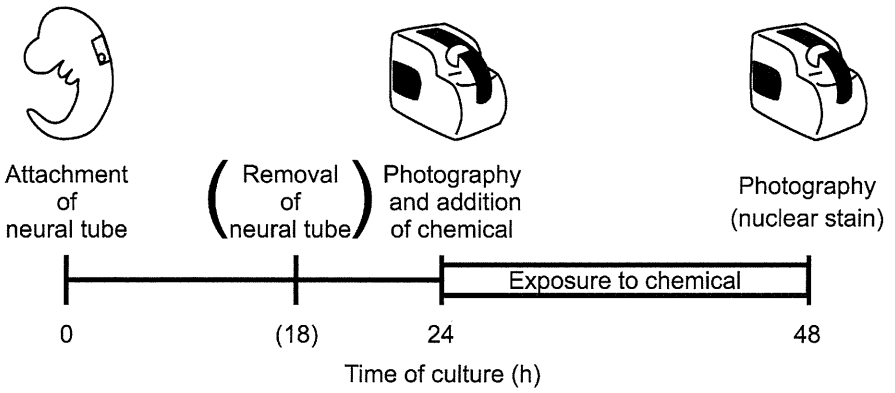

Fig. 1

CGA_12121_F1

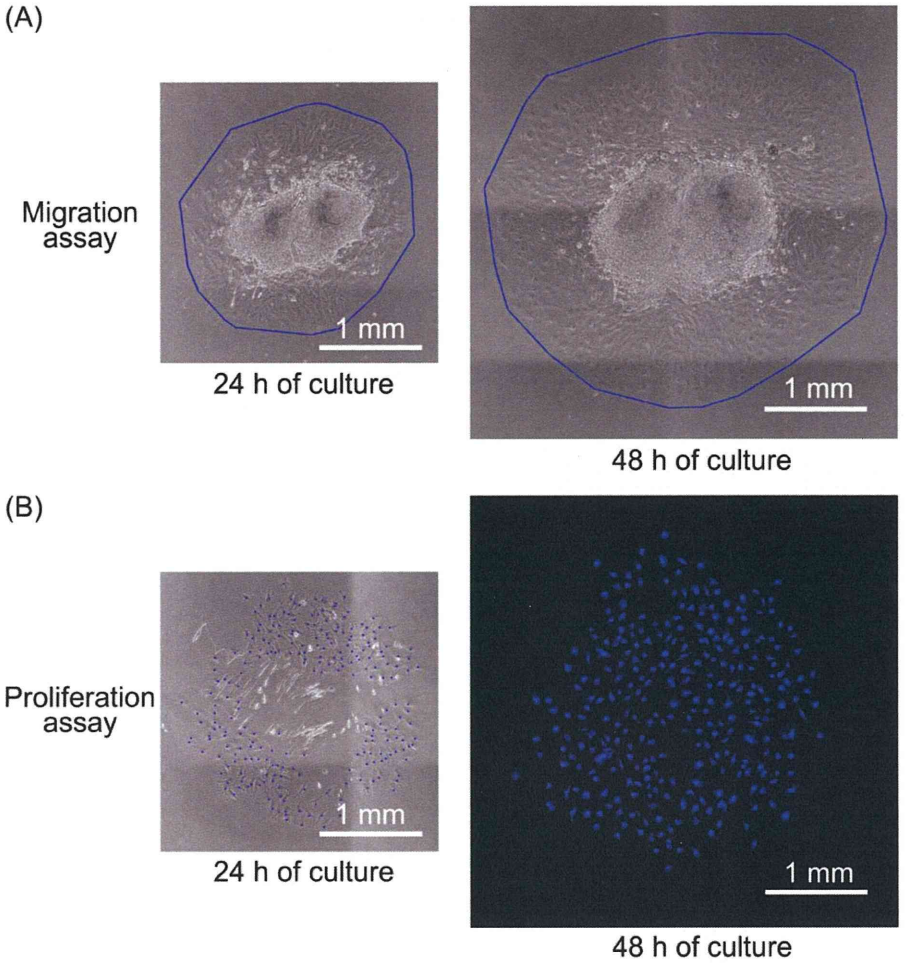

Fig.2

CGA_12121_F2

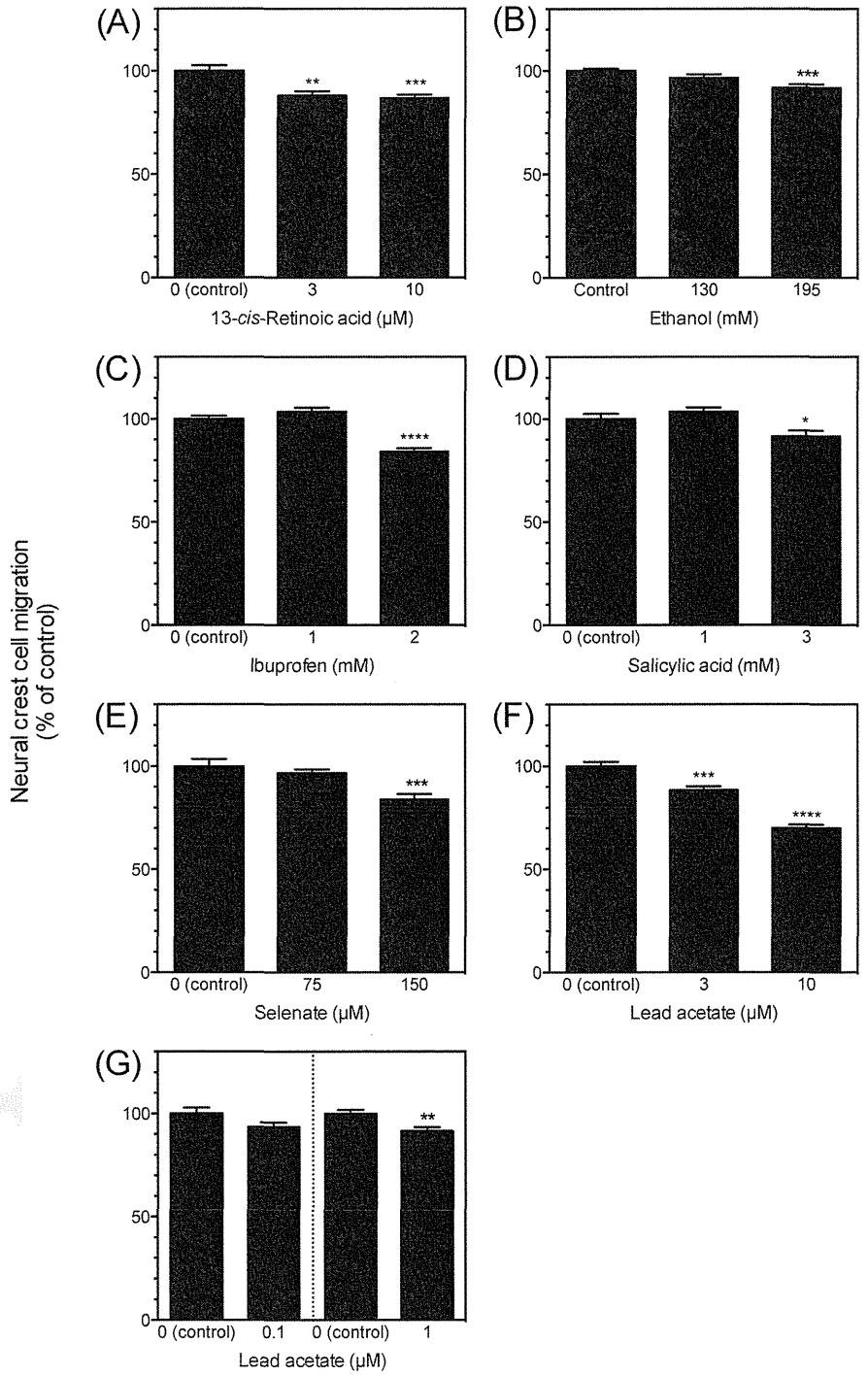

Fig.3

CGA_12121_F3

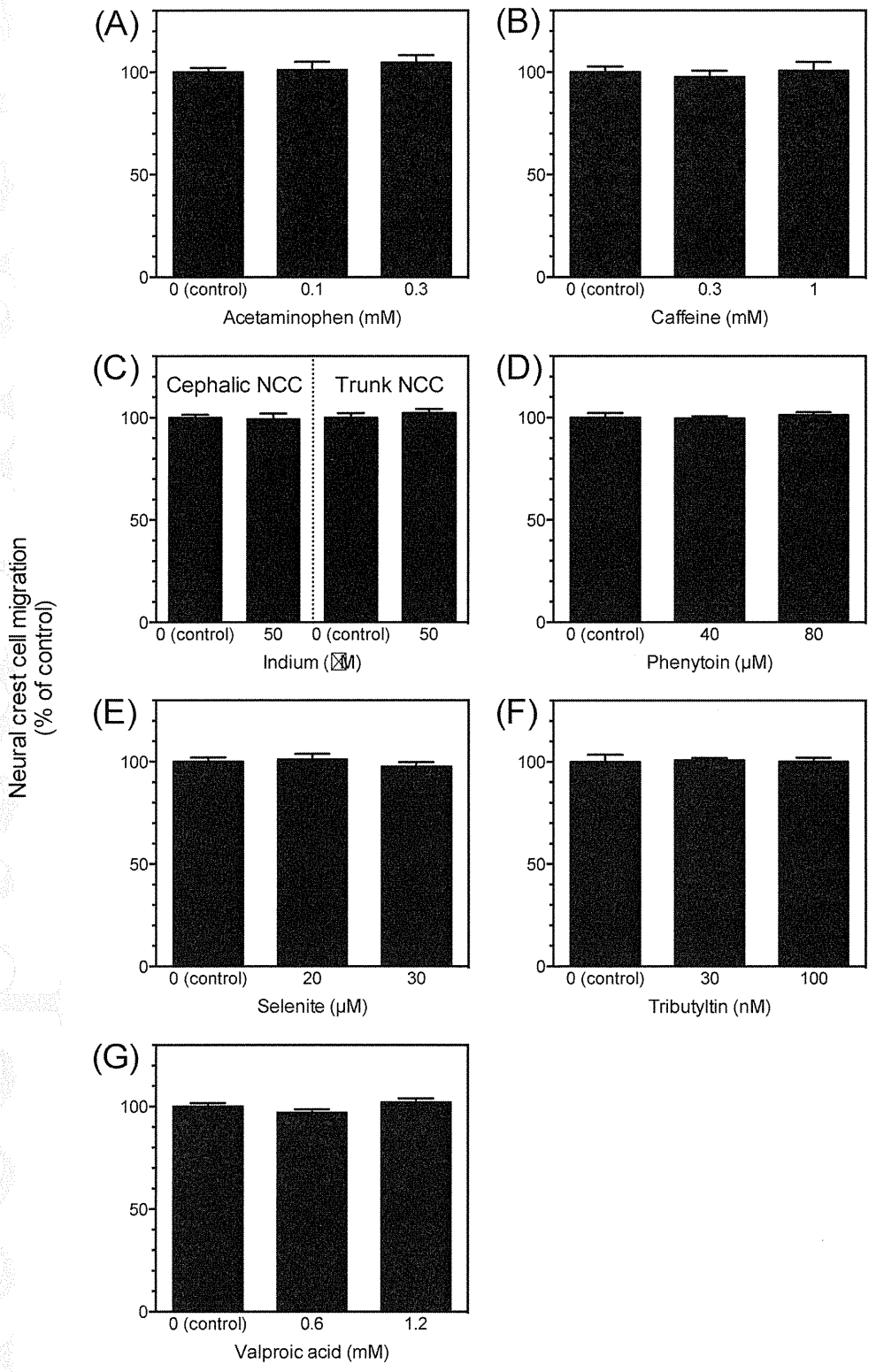

Fig.4

CGA_12121_F4

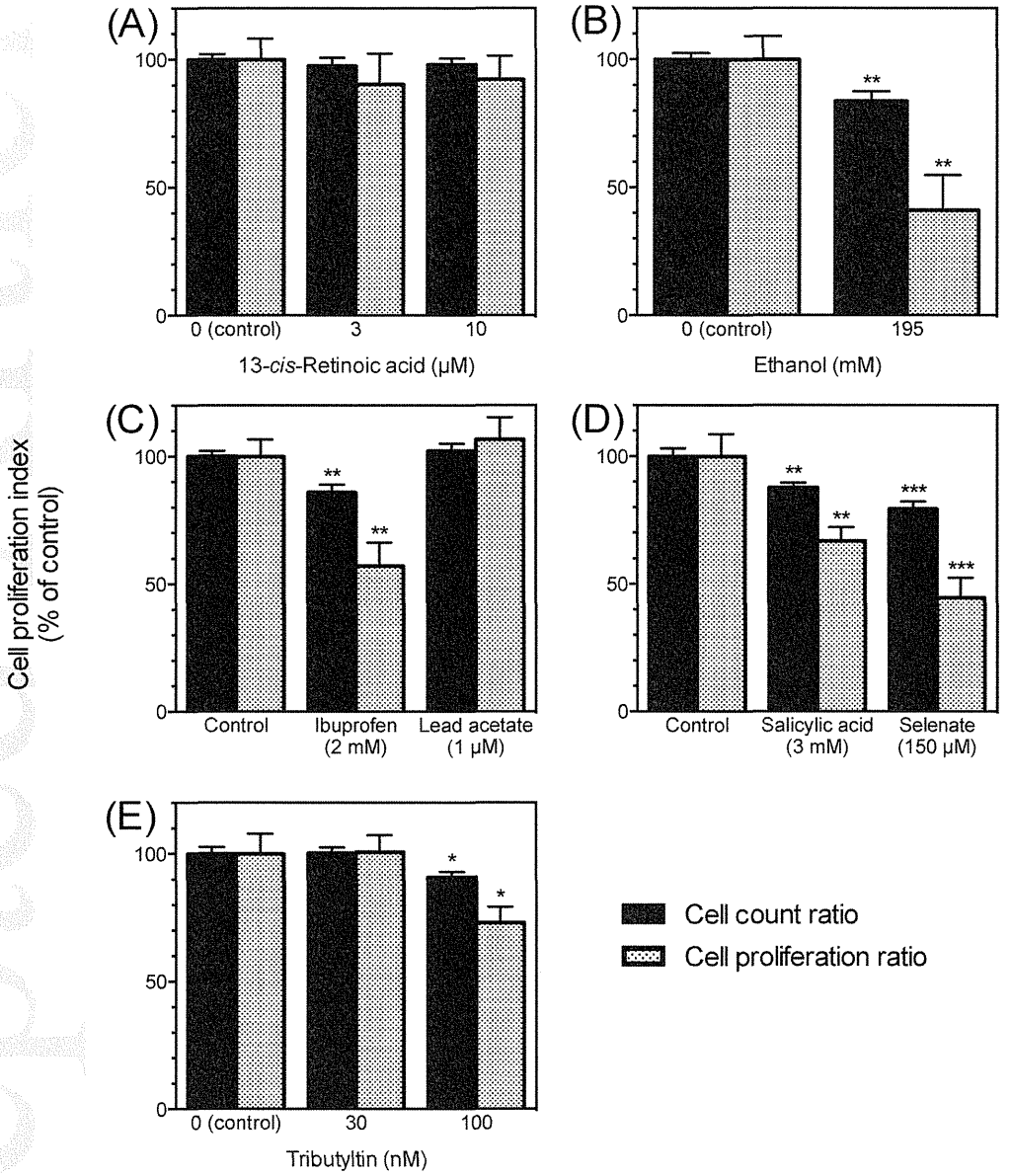

Fig.5

CGA_12121_F5

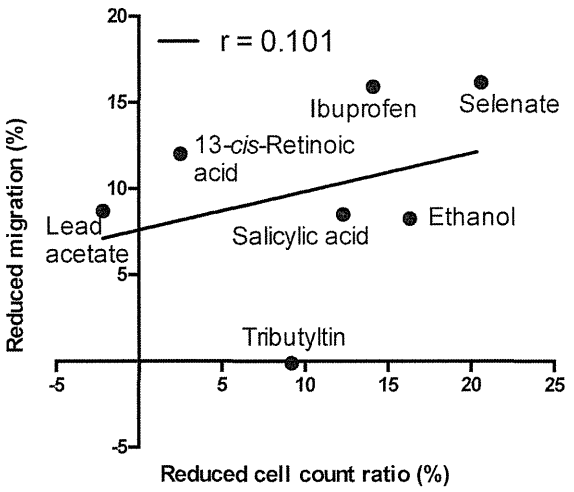

Fig.6

CGA_12121_F6

Neuropharmacology 95 (2015) 479–491

Contents lists available at ScienceDirect

Neuropharmacology

journal homepage: www.elsevier.com/locate/neuropharm

MAM-2201, a synthetic cannabinoid drug of abuse, suppresses the synaptic input to cerebellar Purkinje cells via activation of presynaptic CB1 receptors

Tomohiko Irie [a, *], Ruri Kikura-Hanajiri [b], Makoto Usami [a], Nahoko Uchiyama [b], Yukihiro Goda [c], Yuko Sekino [a, **]

[a] Division of Pharmacology, National Institute of Health Sciences, Tokyo, Japan
[b] Division of Pharmacognosy, Phytochemistry, and Narcotics, National Institute of Health Sciences, Tokyo, Japan
[c] Division of Drugs, National Institute of Health Sciences, Tokyo, Japan

ARTICLE INFO

Article history:
Received 26 June 2014
Received in revised form
18 December 2014
Accepted 20 February 2015
Available online 5 March 2015

Keywords:
Synthetic cannabinoids
MAM-2201
Cannabinoid receptor type 1
Purkinje cell
Cerebellum
Neurotransmitter release

ABSTRACT

Herbal products containing synthetic cannabinoids—initially sold as legal alternatives to marijuana—have become major drugs of abuse. Among the synthetic cannabinoids, [1-(5-fluoropentyl)-1*H*-indol-3-yl](4-methyl-1-naphthalenyl)-methanone (MAM-2201) has been recently detected in herbal products and has psychoactive and intoxicating effects in humans, suggesting that MAM-2201 alters brain function. Nevertheless, the pharmacological actions of MAM-2201 on cannabinoid receptor type 1 (CB1R) and neuronal functions have not been elucidated. We found that MAM-2201 acted as an agonist of human CB1Rs expressed in AtT-20 cells. In whole-cell patch-clamp recordings made from Purkinje cells (PCs) in slice preparations of the mouse cerebellum, we also found that MAM-2201 inhibited glutamate release at parallel fiber-PC synapses via activation of presynaptic CB1Rs. MAM-2201 inhibited neurotransmitter release with an inhibitory concentration 50% of 0.36 μM. MAM-2201 caused greater inhibition of neurotransmitter release than Δ^9-tetrahydrocannabinol within the range of 0.1–30 μM and JWH-018, one of the most popular and potent synthetic cannabinoids detected in the herbal products, within the range of 0.03–3 μM. MAM-2201 caused a concentration-dependent suppression of GABA release onto PCs. Furthermore, MAM-2201 induced suppression of glutamate release at climbing fiber-PC synapses, leading to reduced dendritic Ca^{2+} transients in PCs. These results suggest that MAM-2201 is likely to suppress neurotransmitter release at CB1R-expressing synapses in humans. The reduction of neurotransmitter release from CB1R-containing synapses could contribute to some of the symptoms of synthetic cannabinoid intoxication including impairments in cerebellum-dependent motor coordination and motor learning.

Abbreviations: ACSF, artificial cerebrospinal fluid; AM251, *N*-(piperidin-1-yl)-5-(4-iodophenyl)-1-(2,4-dichlorophenyl)-4-methyl-1*H*-pyrazole-3-carboxamide; CB1R, cannabinoid receptor type 1; CB2R, cannabinoid receptor type 2; CF, climbing fiber; CI, confidence interval; CV, coefficient of variation; DNQX, 6,7-dinitroquinoxaline-2,3-dione; EC50, effective concentration 50%; eCBs, endocannabinoids; EGTA, ethylene glycol tetraacetic acid; EPSC, excitatory postsynaptic current; GFP, green fluorescent protein; hCB1R, human CB1R; HEPES, 4-(2-hydroxyethyl)-1-piperazineethanesulfonic acid; IC50, inhibitory concentration 50%; IEI, inter-event interval; IPSC, inhibitory postsynaptic current; JWH-018, naphthalen-1-yl-(1-pentylindol-3-yl)methanone; LTD, long-term depression; MAM-2201, [1-(5-fluoropentyl)-1*H*-indol-3-yl](4-methyl-1-naphthalenyl)-methanone; mCB1R, mouse CB1R; mIPSC, miniature IPSC; OGB-1, Oregon Green 488 BAPTA-1 hexapotassium salt; P, postnatal day; PC, Purkinje cell; PF, parallel fiber; PPR, paired-pulse ratio; qEPSC, quantal EPSC; THC, tetrahydrocannabinol; TTX, tetrodotoxin; WIN, WIN 55,212-2 mesylate, (*R*)-(+)-[2,3-Dihydro-5-methyl-3-(4-morpholinylmethyl)pyrrolo[1,2,3-de]-1,4-benzoxazin-6-yl]-1-naphthalenylmethanone mesylate.

* Corresponding author. Division of Pharmacology, National Institute of Health Sciences, 1-18-1 Kamiyoga, Setagaya-ku, Tokyo 158-8501, Japan. Tel.: +81 3 3700 9762.
** Corresponding author. Division of Pharmacology, National Institute of Health Sciences, 1-18-1 Kamiyoga, Setagaya-ku, Tokyo 158-8501, Japan. Tel.: +81 3 3700 9692.
E-mail addresses: irie@nihs.go.jp (T. Irie), yukos@nihs.go.jp (Y. Sekino).

http://dx.doi.org/10.1016/j.neuropharm.2015.02.025
0028-3908/

1. Introduction

Marijuana (*Cannabis sativa*) has been widely abused for recreational purposes and contains the psychoactive compound Δ^9-tetrahydrocannabinol (Δ^9-THC) (Taura et al., 2007). Δ^9-THC binds to cannabinoid receptors type 1 and 2 (CB1R and CB2R), which are G protein-coupled receptors. CB1Rs are abundantly expressed in the mammalian brain, whereas CB2Rs are expressed mainly in the immune system (Showalter et al., 1996; Mackie, 2008; Kano et al., 2009). The psychoactive effects of Δ^9-THC are mediated by CB1Rs (Huestis et al., 2001; Monory et al., 2007). Starting in the late 2000s, herbal products containing synthetic cannabinoids, which are chemical compounds produced for the purpose of mimicking the effects of Δ^9-THC, became a major class of drugs of abuse, and are sold as alternatives to marijuana around the world (Auwarter et al., 2009; Vardakou et al., 2010; Seely et al., 2012; Kikura-Hanajiri et al., 2013). Among the synthetic cannabinoids, [1-(5-fluoropentyl)-1*H*-indol-3-yl](4-methyl-1-naphthalenyl)-methanone (MAM-2201, Fig. 1*A*) was recently identified in these herbal products (Moosmann et al., 2012; Derungs et al., 2013; Kikura-Hanajiri et al., 2013; Saito et al., 2013; Uchiyama et al., 2013; Lonati et al., 2014). In humans, abuse of products containing MAM-2201 causes a psychotic state with agitation, aggression, and anxiety, and can cause serious harm to the user including death. These reports imply that MAM-2201 exerts potent pharmacological actions on brain functions and causes psychoactive and intoxicating effects. Nevertheless, it remains unknown whether MAM-2201 activates CB1Rs and how MAM-2201 affects neuronal functions such as synaptic transmission.

Endocannabinoids (eCBs) mediate various types of synaptic plasticity throughout the mammalian brain. eCBs are released from postsynaptic neurons in response to synaptic activity and act in a retrograde manner on presynaptic terminals, to suppress neurotransmitter release (Wilson and Nicoll, 2002; Kano et al., 2009; Regehr et al., 2009). The synaptic effects of eCBs are mediated by presynaptic CB1Rs. In presynaptic terminals, activation of CB1Rs mainly inhibits voltage-gated Ca^{2+} channels coupled to exocytosis, leading to a reduction of neurotransmitter release (Brown et al., 2004; Kushmerick et al., 2004).

Numerous neurophysiological and neuropharmacological studies of CB1Rs have been performed on the cerebellum of rodents, which have well-characterized neuronal circuits and play crucial roles in motor coordination and motor learning (Llinas et al., 2004; Kano et al., 2009). In the cerebellum, Purkinje cells (PCs) are the principal GABAergic neurons and provide the sole output from the cerebellar cortex. PCs receive two types of glutamatergic excitatory inputs, climbing fibers (CFs) and parallel fibers (PFs). CFs arise from the inferior olivary complex. Activation of CF-PC synapses induces strong postsynaptic depolarization, which evokes a dendritic Ca^{2+} transient and complex spikes consisting of a burst of several action potentials (spikelets). PFs are the axons of the granule cells located in the deep layers of the cerebellum and form numerous *en passant* synapses on the spines of distal dendrites of PCs (Llinas et al., 2004). PCs also receive feed-forward inhibition from GABAergic interneurons in the molecular layer of the cerebellar cortex (Mittmann et al., 2005). Neurotransmitter release at CF-PC, PF-PC, and interneuron-PC synapses is suppressed via activation of presynaptic CB1Rs (Kreitzer and Regehr, 2001; Diana et al., 2002; Szabo et al., 2004; Kawamura et al., 2006; Safo et al., 2006). *In vivo* administration of synthetic CB1R agonists in mice impairs cerebellum-dependent motor coordination (DeSanty and Dar, 2001; Patel and Hillard, 2001). Thus, the effects of CB1R agonists on cerebellar functions are well understood. Therefore, the cerebellum is the ideal neuronal circuit to examine the potency of synthetic cannabinoids, whose actions on neuronal functions have not been determined.

Here, using whole-cell patch-clamp recordings, we investigated activity of MAM-2201 in human CB1R (hCB1R)-expressing AtT-20 cells, and then the effects of MAM-2201 on synaptic transmission in slice preparations of the mouse cerebellum. We found that MAM-2201 acted as an agonist of hCB1Rs and inhibited excitatory transmitter release at PF-PC synapses via activation of presynaptic CB1Rs. MAM-2201 decreased the synaptic transmission more strongly than Δ^9-THC within the range of 0.1–30 μM and naphthalen-1-yl-(1-pentylindol-3-yl)methanone [JWH-018, Fig. 1*B*, one of the most popular and potent synthetic cannabinoids detected in the herbal products (Atwood et al., 2010)], within the range of 0.03–3 μM. Furthermore, MAM-2201 induced presynaptic suppression of CF-PC synapses, leading to a reduction in the number of spikelets in complex spikes and to attenuated dendritic Ca^{2+} transients in PCs.

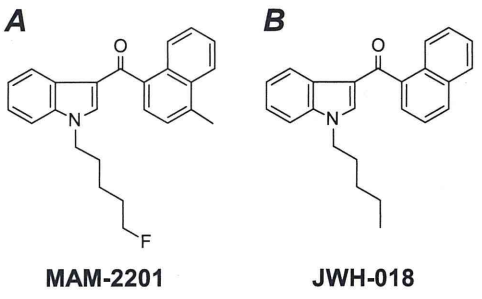

Fig. 1. The chemical structures of [1-(5-fluoropentyl)-1*H*-indol-3-yl](4-methyl-1-naphthalenyl)-methanone (MAM-2201, *A*) and naphthalen-1-yl-(1-pentylindol-3-yl) methanone (JWH-018, B).

2. Materials and methods

2.1. Cannabinoid-related compounds

MAM-2201 (Fig. 1*A*) and JWH-018 (Fig. 1*B*) were purchased from Cayman Chemical (Ann Arbor, MI, USA). (*R*)-(+)-[2,3-Dihydro-5-methyl-3-(4-morpholinylmethyl)pyrrolo[1,2,3-de]-1,4-benzoxazin-6-yl]-1-naphthalenylmethanone mesylate [WIN55,212-2 (WIN), a CB1R and CB2R agonist] and *N*-(Piperidin-1-yl)-5-(4-iodophenyl)-1-(2,4-dichlorophenyl)-4-methyl-1*H*-pyrazole-3-carboxamide (AM251, a CB1R antagonist) were purchased from Wako Pure Chemical Industries (Osaka, Japan) and Tocris Bioscience (Bristol, UK), respectively. Δ^9-THC was purchased from Cerilliant (Round Rock, TX, USA). These compounds were dissolved in dimethylsulfoxide as stock solutions. In electrophysiological recordings from AtT-20 cells and from cerebellar PCs, the final concentrations of dimethylsulfoxide in extracellular solutions were maintained at 0.1 and 0.3% (v/v), respectively. WIN was used as a positive control, because WIN has been used in many studies to suppress neurotransmitter release at PF-, CF-, and interneuron-PC synapses via activation of presynaptic CB1Rs (Kreitzer and Regehr, 2001; Diana et al., 2002; Safo and Regehr, 2005; Kawamura et al., 2006).

2.2. Heterologous expression of CB1R in AtT-20 cells

AtT-20 cells were obtained from JCRB Cell Bank (Osaka, Japan) and were maintained in Ham's F-10 medium (GIBCO, Grand Island, NY) supplemented with 10% horse serum (GIBCO), 2.5% fetal bovine serum (GIBCO), and a mixture of penicillin and streptomycin solution (100 unit/mL and 100 mg/mL, respectively; GIBCO) in a 5% CO_2 incubator at 37 °C. The cells were plated onto grass coverslips coated with poly-D-lysine (Sigma–Aldrich, St Louis, MO) for gene transfection. hCB1R (SC111611; Origene, Rockville, MD; NCBI Reference Sequence: NM_016083.3) (Bruno et al., 2014) or mouse CB1R (mCB1R, MC206086; Origene; GenBank: BC079564.1) cDNAs, and green fluorescent protein (GFP) vector were cotransfected into the cells in a 9:1 M ratio using Lipofectamine LTX (Invitrogen, Carlsbad, CA) according to the manufacturer's instructions. Fluorescence of GFP was regarded as an indicator of transfected cells. Whole-cell patch-clamp recordings were made from the GFP-positive cells 20–48 h after transfection. The expression of CB1R proteins was confirmed by immunostaining with the combination of rabbit polyclonal anti-CB1R antibody (1:2000 dilution, CB1-Rb-Af380, Frontier Institute, Hokkaido, Japan) and AlexaFluor 568-conjugated goat anti-rabbit IgG secondary antibody (5 μg/mL, A-11011; Invitrogen) according to the methods described previously (Irie et al., 2014).

The immunofluorescence signal was observed under a confocal microscope (A1R; Nikon, Tokyo, Japan; Fig. 2A).

2.3. Electrophysiological recordings from AtT-20 cells

AtT-20 cells were transferred to a recording chamber and continuously perfused at 2 mL/min with high-K^+ extracellular solution containing (in mM): 87 NaCl, 60 KCl, 2 $CaCl_2$, 1 $MgCl_2$, 10 D-glucose, and 10 4-(2-hydroxyethyl)-1-piperazineethanesulfonic acid (HEPES) (pH adjusted to 7.4 with NaOH). The concentration of KCl was raised compared to normal extracellular solution to increase amplitudes of inwardly rectifier potassium currents (Mackie et al., 1995). All experiments were performed at 25 ± 1 °C. The cells were visualized by Nomarski optics and a near infrared-CCD camera (C3077-79; Hamamatsu Photonics, Hamamatsu, Japan) with a 40 × 0.8 NA numerical aperture water-immersion objective lens (Olympus, Tokyo, Japan) on an upright microscope (BX51WI; Olympus). GFP-positive cells were visualized and selected using epifluorescence optics (Olympus).

Patch pipettes were made from borosilicate glass capillaries (GC150F-100; Harvard Apparatus, Holliston, MA) and had a resistance of 3–5 MΩ when filled with a potassium gluconate-based internal solution containing (in mM): 125 K-gluconate, 10 KCl, 3 $MgCl_2$, 0.1 ethylene glycol tetraacetic acid (EGTA), 5 Na_2-ATP, 5 Na_2-phosphocreatine, 0.3 Na_2-GTP, and 10 HEPES (pH adjusted to 7.3 with KOH). Whole-cell patch-clamp recordings were performed from GFP-positive cells, and inward currents were evoked by applying voltage steps from a holding potential of −25 mV to −110 mV for 200 ms in voltage-clamp conditions. Membrane capacitance was calculated from the transient current evoked by applying a small voltage step (−5 mV, 20 ms duration) from a holding potential of −25 mV (Irie et al., 2006). Series resistance was compensated electronically by 70–90%, and the liquid junction potential (−5 mV) was corrected off-line.

Data were collected with Molecular Devices (Sunnyvale, CA) hardware and software (Multiclamp 700B, Digidata 1440A, Clampex 10.3) as described previously (Irie et al., 2014), and analyzed using Clampfit 10.3 software (Molecular Devices) and Igor Pro 6 software (Wavemetrics, Lake Oswego, OR) with the added import functionality provided by ReadPclamp XOP of the NeuroMatic software package (http://www.neuromatic.thinkrandom.com/). Representative current traces are shown after averaging four consecutive traces. To obtain inward current densities induced by MAM-2201 or WIN, the amplitudes of the current were normalized to membrane capacitances (picoamperes per picofarad, Fig. 2C). The densities were plotted as a function of the concentration and fit with the sigmoidal function, $Y = Bottom + (Top - Bottom)/(1 + 〖10〗^{(LogEC50 - X)*Hillslope})$, using GraphPad Prism 5 (GraphPad Software, San Diego, CA).

2.4. Cerebellar slice preparation and electrophysiological recordings from PCs

ICR mice of either sex [postnatal day (P) 20–57 for Figs. 3–5 and Table 1; P14–20 for Figs. 6 and 7, and Table 2] were used according to the guidelines for animal use of the National Institute of Health Sciences. Cerebellar slices were prepared as described previously with some modifications (Shuvaev et al., 2011). Briefly, mice were anesthetized with halothane and decapitated. Parasagittal slices of the cerebellum (200-μm thick) were prepared using a microslicer (PRO7, Dosaka, Kyoto, Japan) in ice-cold, cutting solution containing (in mM): 234 sucrose, 2.5 KCl, 1.25 NaH_2PO_4, 10 $MgSO_4$, 0.5 $CaCl_2$, 26 $NaHCO_3$, 11 glucose, and bubbled with 5% CO_2/95% O_2. The slices were then allowed to recover for 1 h at room temperature in artificial cerebrospinal fluid (ACSF) solution containing (in mM): 120 NaCl, 2.5 KCl, 2 $CaCl_2$, 1 $MgCl_2$, 1.25 NaH_2PO_4, 26 $NaHCO_3$, 17 glucose, 0.4 ascorbic acid, 3 myo-inositol, 2 sodium pyruvate, and bubbled with 5% CO_2/95% O_2. In electrophysiological recordings, ascorbic acid, myo-inositol, and sodium pyruvate were omitted.

Cerebellar slices were transferred to a recording chamber, and continuously perfused at 2 mL/min with ACSF at 25 ± 1 °C (Figs. 3–6 and Table 1) or near physiological temperature (34 ± 1 °C; Fig. 7 and Table 2). Electrophysiological recordings were done using the same equipment described above. Excitatory and inhibitory postsynaptic currents (EPSCs and IPSCs) were recorded in the presence of 100 μM picrotoxin (a $GABA_A$ receptor antagonist, Tocris Bioscience) and 40 μM 6,7-dinitroquinoxaline-2,3-dione (DNQX, an AMPA/kainate receptor antagonist, Tocris Bioscience), respectively. Patch pipettes had a resistance of 2–3 MΩ when filled with pipette solutions. A CsCl-based and the K-gluconate-based internal solutions were used for voltage- (Figs. 3–6 and Table 1) and current-clamp recordings (Fig. 7 and Table 2), respectively. The CsCl-based solution contained (in mM): 120 CsCl, 20 K-gluconate, 15 tetraethylammonium-Cl, 3 $MgCl_2$, 5 EGTA, 5 Na_2-ATP, 5 Na_2-phosphocreatine, 0.3 Na_2-GTP, 5 QX-314, and 10 HEPES (pH adjusted to 7.3 with CsOH). The liquid junction potentials (CsCl-based, −4 mV; K-gluconate-based, −10 mV) were corrected off-line.

Somatic whole-cell patch-clamp recordings were performed from PCs in lobules IV to VIII. PF-PC EPSCs and IPSCs were evoked by electrical stimulation of the molecular layer and recorded at the holding potential of −80 mV. CF-PC EPSCs and complex spikes were evoked by the stimulation of the granule cell layer. CF-PC EPSCs were recorded at a holding potential of −10 mV to decrease the driving force for cations through ionotropic glutamate receptors. The stimuli (100- to 200-μs pulses, 20–80 V amplitude) were performed with an ACSF-filled patch pipette (tip diameter, 10–15 μm for molecular layer stimulation and 2–3 μm for the granule cell layer) and applied at 0.1 Hz. In some experiments, paired-pulse stimulation (50 ms inter-stimulus intervals) was done to calculate the paired-pulse ratio (PPR), which is an index of the change of neurotransmitter release from presynaptic terminals (Zucker and Regehr, 2002; Irie and Ohmori, 2008). When postsynaptic currents were recorded, series resistance was monitored by applying small voltage steps (−10 mV, 20-ms duration), and the records were discarded if the resistance varied more than 25%. Quantal EPSCs (qEPSCs) from PFs and CFs were elicited by electrical stimulation (0.1 Hz) with PCs held at −80 mV and with $CaCl_2$ in ACSF replaced with equimolar $SrCl_2$ (Xu-Friedman and Regehr, 1999). Miniature IPSCs (mIPSCs) were recorded at a holding potential of −80 mV in the presence of 40 μM DNQX and 1 μM tetrodotoxin (TTX; Wako Pure Chemical Industries). In the start of current-clamp recordings, resting membrane potentials of PCs were adjusted at −60 to −70 mV by current injection to prevent spontaneous firing, and series resistance was compensated for using bridge balance and capacitance neutralization. Intrinsic membrane properties were examined by square-wave current injection (500-ms duration, Table 2). Input resistance was measured from averaged voltage responses evoked by small hyperpolarizing currents (−20 pA). Threshold current and threshold potential were measured by depolarizing current injections (from 0 pA to 200 pA, 20 pA increment). The maximum rate of rise and maximum rate of fall of action potentials and spike height were calculated from the first action potential waveform evoked at the threshold current. Firing frequency was obtained from the number of spikes observed during the current injection.

qEPSCs and mIPSCs were detected off-line using the template search function in the Clampfit 10.3 software. To analyze qEPSCs, data from 200 to 1600 ms after the stimulus artifact were used. Average cumulative probability histograms were obtained as follows: first, qEPSCs or mIPSCs were recorded more than 300 events from each cell in the presence or absence of MAM-2201. Then, for each cell, the amplitudes and inter-event intervals were binned, and individual cumulative probability histograms were plotted. Finally, these histograms were averaged. Representative EPSC and IPSC traces are shown after averaging four to six consecutive traces, and stimulus artifacts are truncated. EPSC and IPSC amplitudes were obtained by averaging six consecutive records. The coefficient of variation (CV), which is another index of the change of neurotransmitter release from presynaptic terminals, was calculated from 18 consecutive EPSC or IPSC traces (Korn and Faber, 1991). The inhibitory concentration 50% (IC50) values of the cannabinoid-related compounds against neurotransmitter release at PF-PC synapses were calculated as follows: control PF-PC EPSC amplitude was obtained from the averaged EPSCs recorded for 3 min before application of the synthetic cannabinoids. PF-PC EPSC amplitude in the presence of the cannabinoids was done from the EPCSs recorded for 8 to 10 min after the application, normalized to the control values, and plotted as a function of the concentration. The data were fit with the sigmoidal function, $Y = 100/(1 + 〖10〗^{(LogIC50 - X)*Hillslope})$ (Table 1). The reasons for using PF-PC synapses for measurement of IC50s were as follows: PF-PC synapses exhibit more stable synaptic transmission than interneuron-PC synapses (Vincent and Marty, 1996), they are more sensitive to CB1R agonists, and they express CB1R proteins more abundantly than CF-PC synapses (Kawamura et al., 2006).

2.5. Simultaneous recordings of Ca^{2+} transients and complex spikes

Current-clamp recordings were done from PCs using the K-gluconate-based intracellular solution in which EGTA was replaced with 100 μM Oregon Green 488 BAPTA-1 hexapotassium salt (OGB-1; Invitrogen, Carlsbad, CA) in the presence of picrotoxin. PC somata and dendrites were dialyzed with the pipette solution for 30 min to obtain a stable intracellular concentration of OGB-1. Confocal imaging was then performed with a Nipkow disk confocal scanner unit (CSU-10; Yokogawa Electric, Tokyo, Japan) attached to the Olympus BX51WI microscope with the 40× objective lens. A 488 nm beam from a diode laser (Yokogawa Electric) for excitation was coupled to the scanner unit through an optical fiber. Fluorescence was detected via a 520 nm long-path filter using an EMCCD camera (iXon3 DU897; Andor Technology, Belfast, Northern Ireland). The pixels were binned 2 × 2 on the chip, and images were acquired at 25.8 Hz. Complex spikes were evoked at 0.1 Hz, and the electrophysiological recordings were synchronized with the acquisition of time-lapse fluorescent images. The number of spikelets in complex spikes was obtained from average value of five to seven consecutive traces. The imaging experiments were controlled and analyzed using Andor iQ2 software (Andor Technology). Three to five consecutive time-lapse images were averaged and used for analysis. The regions of interests were set on primary dendrites (approximately between 20 and 100 μm from the center of the cell body, Fig. 7Ca). Fluorescence changes were background-corrected and expressed as $\Delta F/F_0$, where F_0 is the fluorescence intensity when the cells were at rest, and ΔF is the absolute values of fluorescence changes during activity. Integration of Ca^{2+} transients was performed over 2 s from the onset.

All data other than EC50s or IC50s are provided as the means ± standard deviation. EC50s and IC50s are expressed as the best-fit values with 95% confidence interval (CI; Table 1). *n* indicates the number of experiments. Statistical significance was tested using paired *t*-tests test unless otherwise stated (significance, $p < 0.05$).

3. Results

3.1. MAM-2201 acts as an agonist of hCB1Rs and mCB1Rs

To examine whether MAM-2201 activates CB1Rs, we expressed hCB1R or mCB1R cDNAs in murine tumor line AtT-20. Because

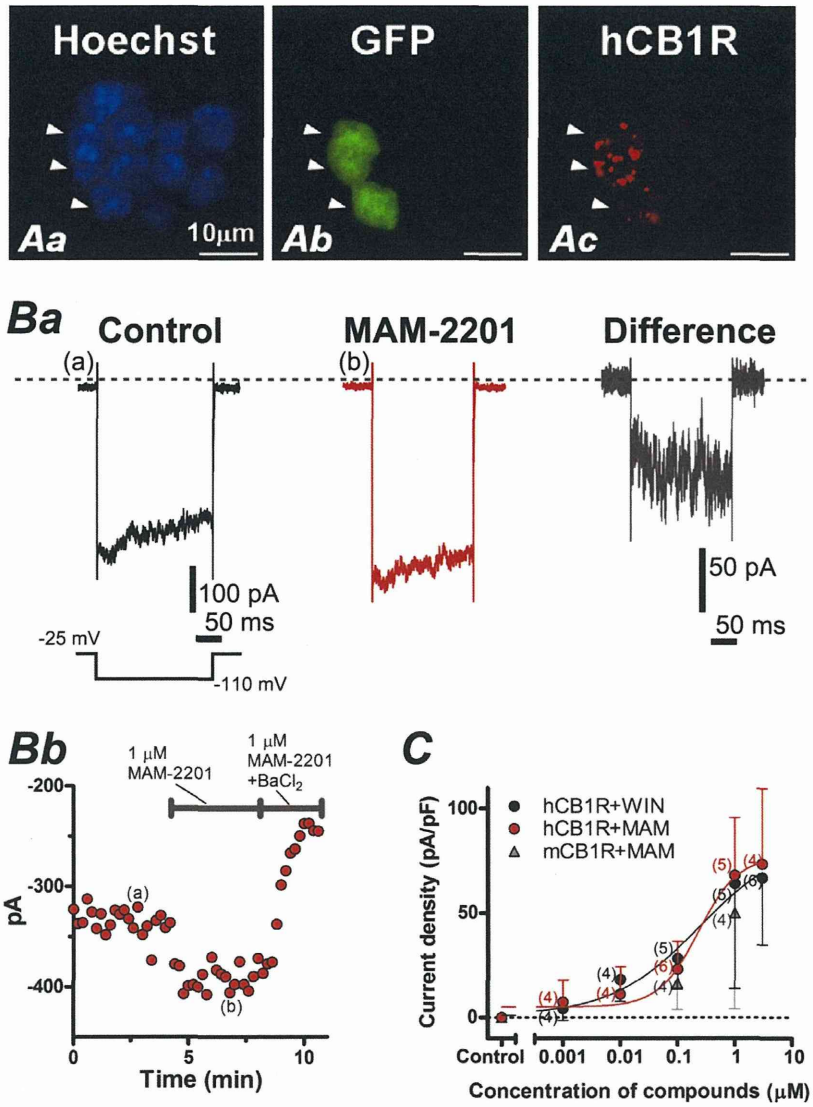

Fig. 2. Heterologous expression of cannabinoid receptor type 1 (CB1R) cDNAs in AtT-20 cells. A, Immunofluorescence images of AtT-20 cells transfected with human CB1R (hCB1R) and green fluorescent protein (GFP) cDNAs. Cell nuclei were stained with Hoechst 33342 (1 μg/mL, Dojindo, Kumamoto, Japan; Aa). Arrowheads indicate GFP and hCB1R double positive cells. Proteins of hCB1Rs were visualized by immunolabelling with rabbit anti-CB1R antibody and AlexaFluor 568-conjugated anti-rabbit secondary antibody (Ac). B, Representative data recorded from hCB1R-expressing cell. Ba, Inward currents were evoked by applying voltage steps from a holding potential of −25 mV to −110 mV for 200 ms. In trace (a) and (b), averages of four consecutive responses are shown. These traces correspond to the responses at time points marked (a) or (b) in Bb. The holding current level is shown by a dotted line. Bb, Time course of mean inward currents. Each point represents an averaged value obtained from four consecutive records. C, Concentration-dependent increases of inward current densities induced by MAM-2201 or (*R*)-(+)-[2,3-Dihydro-5-methyl-3-(4-morpholinylmethyl)pyrrolo[1,2,3-de]-1,4-benzoxazin-6-yl]-1-naphthalenylmethanone mesylate [WIN55,212-2 (WIN)]. To obtain current densities, amplitudes of inward current induced by MAM-2201 or WIN were normalized to membrane capacitances (picoamperes per picofarad). The densities were plotted as a function of the concentration and fit with the sigmoidal function, Y = Bottom + (Top − Bottom)/(1 + ⟦10⟧ ⁅(LogEC50 − X)*Hillslope⁆), where EC50 is effective concentration 50%. Here and in the following figures, error bars and the numbers in parentheses indicate standard deviation and the number of experiments, respectively.

application of CB1 agonists on AtT-20 cells expressing CB1Rs activates inward rectifier potassium currents, activities of compounds against CB1Rs can be determined using this heterologous expression system (Mackie et al., 1995; Felder et al., 1998). Whole-cell patch clamp recordings were done from hCB1R or mCB1R-expressing cells, and inward currents were evoked by applying hyperpolarizing voltage pulses (Fig. 2*B*). Bath application of MAM-2201(1 μM) increased the amplitude of inward current within 5 min (Fig. 2*Bb*). Subsequent application of low concentration of Ba^{2+} (200 μM $BaCl_2$), which blocks inward rectifier potassium currents (Hagiwara et al., 1976), markedly reduced the inward currents. This indicates that, in addition to MAM-2201-induced currents, MAM-2201-independent inward rectifier potassium currents were simultaneously blocked (Dousmanis and Pennefather, 1992). The time course of the induced current, obtained by subtracting the currents before from those after the application of MAM-2201, showed slow activation at the beginning of voltage pulse (Fig. 2*Ba*, Difference). This property is characteristic of activation of G-protein coupled potassium channels (Kubo et al., 1993). Fig. 2*C* shows the concentration-dependent increase of current

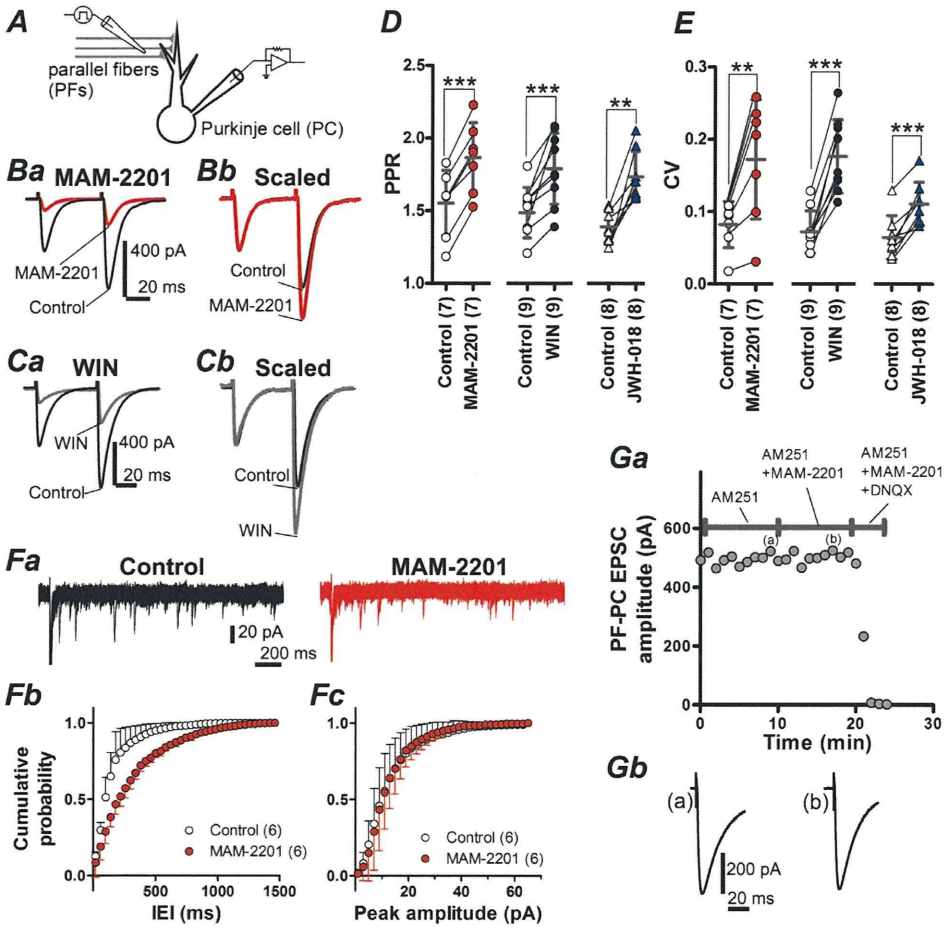

Fig. 3. MAM-2201 inhibits synaptic transmission at parallel fiber (PF)-Purkinje cell (PC) synapses presynaptically via activation of presynaptic CB1Rs. *A*, Experimental configuration for Fig. 3*B*–*G* and 4. *B*, PF-induced excitatory postsynaptic currents (EPSCs) were evoked with pairs of stimuli (50 ms interval) under control conditions (Control) or in the presence of 10 μM MAM-2201 (MAM-2201). The holding potential was −80 mV. Picrotoxin (100 μM) was added to the extracellular artificial cerebrospinal fluid (ACSF) to block $GABA_A$ receptor-mediated inhibitory postsynaptic currents (IPSCs). The first EPSC peak in MAM-2201 was reduced to 21.9% of control. In each trace, averages of six trials are shown. In the right panel, the EPSC evoked by the first stimulus in MAM-2201 is scaled to the amplitude of the first EPSC in Control. MAM-2201 increased paired-pulse facilitation (*Bb*). Stimulus artifacts are truncated. *C*, Same as in *A*, but in the presence of 10 μM WIN. In *Ca*, the first peak in WIN was reduced to 24.1% of control. In the right panel, the EPSC evoked by the first stimulus in WIN is scaled to the amplitude of the first EPSC in Control. *D* and *E*, Summary of paired-pulse ratio (PPR, *D*) and coefficient of variation (CV, *E*) of PF-PC EPSCs before and after application of MAM-2201, WIN, or JWH-018 (10 μM in all groups). Here and in the following figures, the statistical significance was tested using paired *t*-tests unless otherwise stated (significance, $p < 0.05$). $^{**}p < 0.01$ and $^{***}p < 0.001$. *F*, To isolate quantal EPSCs (qEPSCs) from PFs, asynchronous neurotransmitter release from PF terminals was evoked by stimulating PFs in the presence of Sr^{2+} (2 mM, see Materials and Methods). *Fa*, Five superimposed traces before (Control) and after application of MAM-2201. Asynchronously released quanta are seen as downward current deflections. Synchronous PF-PC EPSCs are truncated. *Fb* and *Fc*, Average cumulative probability histograms of inter-event interval (IEI, *Eb*, bin width: 40 ms) and peak amplitude (*Ec*, bin width: 2 pA) of PF-PC qEPSCs. *Ga*, Time course of peak PF-PC EPSC amplitudes in the presence of *N*-(Piperidin-1-yl)-5-(4-iodophenyl)-1-(2,4-dichlorophenyl)-4-methyl-1*H*-pyrazole-3-carboxamide (AM251, 5 μM). Each point represents an averaged value obtained from six consecutive records. MAM-2201 (10 μM) had no detectable effect on the amplitude. Additional application of 6,7-dinitroquinoxaline-2,3-dione (DNQX, 40 μM) abolished PF-PC EPSCs completely. *Gb*, Traces show normalized PF-PC EPSC responses at time points marked (a) and (b) in *Ga*.

densities induced by MAM-2201 or WIN in CB1R-expressing cells. Interestingly, in hCB1R-expressing cells, MAM-2201 increased current densities in a concentration-dependent manner (Fig. 2*C*, red circles) with an EC50 of 0.230 μM (95% CI, 0.0384–1.37 μM). Similar responses were obtained by application of WIN (Fig. 2*C*, black circles; EC50 = 0.234 μM; 95% CI, 0.410 × 10^{-3}-140 μM), which was consistent with previous report (Mackie et al., 1995). In the presence of AM251 (5 μM, a CB1R antagonist), MAM-2201 (1 μM) did not induce the inward currents (−2.38 ± 7.23 pA/pF, $n = 6$). In cells transfected with GFP alone, MAM-2201 (1 μM) did not elicit any changes (1.55 ± 6.78 pA/pF, $n = 5$). In mCB1R-expressing cells, MAM-2201 induced concentration-dependent increase in the current density (Fig. 2*C*, gray triangles). These results demonstrate that MAM-2201 activates hCB1Rs and mCB1Rs.

3.2. MAM-2201 inhibits synaptic transmission presynaptically via activation of presynaptic CB1Rs at PF-PC synapses in mouse cerebellum

We tested the effects of MAM-2201 on neurotransmitter release at PF-PC synapses and the involvement of CB1Rs (Fig. 3), and compared the potency of MAM-2201 with that of WIN, JWH-018, and Δ^9-THC (Fig. 4 and Table 1). Whole-cell patch-clamp recordings were performed from somata of PCs in mouse cerebellar slices under voltage-clamp conditions, and PF-PC EPSCs were evoked by electrical stimulation of PFs in the molecular layer in the presence of picrotoxin. The recording configuration is illustrated in Fig. 3*A*. As shown in Fig. 3*B*, bath application of MAM-2201 (10 μM, 8 min) significantly decreased the first EPSC amplitude

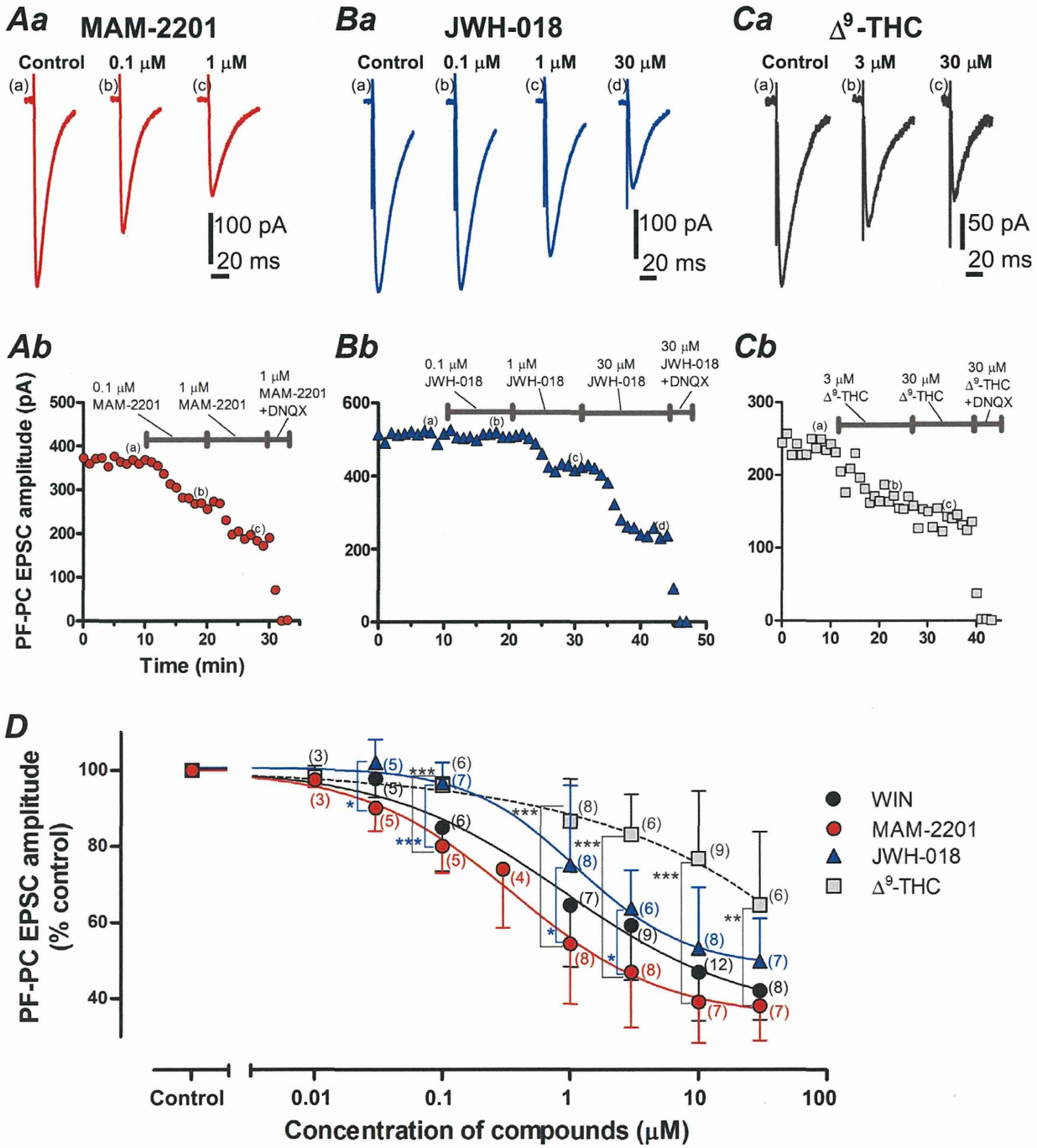

Fig. 4. MAM-2201 is a more potent inhibitor than Δ^9-tetrahydrocannabinol (Δ^9-THC) and JWH-018 at PF-PC synapses. *Aa*, Representative PF-PC EPSC traces recorded in control conditions, or in 0.1 or 1 μM MAM-2201. These traces show normalized PF-PC EPSC responses at time points marked (a), (b), or (c) in *Ab*. *Ab*, Time course of peak amplitudes of PF-PC EPSCs. Each point represents an averaged value obtained from six consecutive records. *Ba*, Representative PF-PC EPSC traces recorded in control conditions, or in 0.1, 1, or 30 μM JWH-018. These traces correspond to the responses at time points marked (a), (b), (c), or (d) in *Bb*. *Bb*, Time course of peak amplitudes of PF-PC EPSCs. *C*, Representative PF-PC EPSC traces recorded in control conditions, or in 3, or 30 μM Δ^9-THC. These traces correspond to the responses at time points marked (a), (b), or (c) in *Cb*. *Cb*, Time course of the peak amplitudes. In *Aa*, *Ba*, and *Ca*, stimulus artifacts are truncated. *D*, Concentration-dependent decreases of PF-PC EPSC amplitudes induced by cannabinoid-related compounds. Control PF-PC EPSC amplitude was obtained from averaged PF-PC EPSCs recorded for 3 min before the application of the compounds. PF-PC EPSC amplitudes in the presence of these compounds were recorded for 8–10 min after application, normalized to the control values, and plotted as a function of concentration (Fig. 4*C*). Each plot was fit with a sigmoidal function, Y = 100/(1 + ⟦10⟧ ⟦(LogIC50 – X)*Hillslope⟧), where IC50 is inhibitory concentration 50%. *$p < 0.05$, **$p < 0.01$, and ***$p < 0.001$ by unpaired *t*-tests test.

(39.0 ± 10.8% of control value, $n = 7$, $p < 0.001$). To investigate whether the effects of MAM-2201 on PF-PC EPSC amplitude were mediated by presynaptic mechanisms, PPR and CV analyses were performed. MAM-2201 (10 μM) significantly increased PPR (Fig. 3*Bb* and *D*) and CV (Fig. 3*E*), indicating a decrease in presynaptic neurotransmitter release. WIN (10 μM, 8-min application) induced a similar decrease in PF-PC EPSC amplitude and a parallel increase in the PPR and CV (Fig. 3*C–E*). MAM-2201 (10 μM) also